An Exact Analytical Model for Near Fields Radiated from Circular Waveguide Antennas

Sameir M. Ali HAMED [1,2]

[1] Dept. of Electronics Engineering, University of Hail, Hail, Kingdom of Saudi Arabia
[2] Dept. of Electrical and Electronics Engineering, Nile Valley University, Atbara, Sudan

sa.hamed@uoh.edu.sa

Submitted June 26, 2026 / Accepted November 6, 2026 / Online first November 20, 2026

Abstract. *This paper introduces new exact expressions for the fields radiated by an open-ended circular waveguide antenna mounted on an infinite ground plane. The method relies on utilizing the equivalence principle and image theory, combined with the Lommel expansions of the scalar Green's function. A direct integration method is subsequently employed to derive the field expressions for the antenna analytically. Simplified expressions for the on-axis and the dominant mode fields are obtained as special cases from the general field expressions. The expressions are valid everywhere in the space surrounding the aperture of the waveguide, on-axis and off-axis, for arbitrary mode and size of the circular waveguide. The field expressions presented in the paper agree very well with the numerical results from the commercial software FEKO and the existing literature's findings, demonstrating the correctness and validity of these field expressions.*

Keywords

Aperture antenna, circular waveguide, far-field, Lommel expansions, near-field, off-axis field, on-axis field

1. Introduction

The open-ended circular waveguide antennas (OECW) are used in many applications as a single element or as an element in array antennas. They are used in reflector antenna systems as feeds, as near-field probes, in near-field focusing technologies, in near-field microwave imaging, and in space exploration systems [1–5] among other applications. On the other hand, knowledge of the antenna's near-field distribution is necessary to assess the level of electromagnetic fields for the purpose of protection against radiation hazards.

Although the far-field radiation properties of these antennas have been extensively studied, the near-field aspect has not received the same level of research and investigation, despite its importance in many of the above applications.

Numerical and analytical techniques have been applied to study the radiation characteristics of the open-ended or truncated circular waveguides including the Method of Moments, Physical Optics (PO), and Wiener-Hopf technique [5–8]. The radiation characteristics of a circular aperture antenna that is flush-mounted on the ground plane, excited by a circular waveguide supporting the dominant mode, and covered by a spherical-shell chiral radome, were analyzed using the dyadic Green function approach [9]. An analytical formulation based on PO along with the incomplete Hankel was employed to determine the field and the radiated power distribution for OECWs [6], [7]. Although these field expressions are exact and valid in the near-field and far-field regions, they apply only on the axis of the waveguide. A generalized procedure for the determination of radiation pattern of antennas, including circular waveguide antennas, at any arbitrary distance which covers both the near-field and far field was presented in [10]. The technique in [10] approximates the equivalent currents on the aperture surface by an array of point dipoles, whose current strength is determined by the field distribution at the respective locations of the dipoles. On the other hand the computation of the radiated fields using this technique requires evaluation of double integrals numerically.

In this paper new exact analytical expressions for the fields radiated from an OECW antennas are derived in a unified approach. The approach is based on the Lommel expansions of the scalar Green's function [11–13] and the direct integration procedure using analytical methods without resorting to any approximations.

The main contribution of this paper is that it provides a generalized analytical exact series expressions for the fields radiated from circular waveguide antennas. The expressions are valid everywhere in the space surrounding the aperture of the waveguide, on-axis and off-axis, for arbitrary mode and size of the circular waveguide. So far, the available solutions for the problem of the circular waveguides radiating in free space are either valid only on the axis of the waveguide [6], [7], or they are based on approximate numerical techniques [10]. Therefore, the solution presented in this pa-

DOI: 10.13164/re.2026.0601

per provides a simple and accurate alternative for calculating the radiated electromagnetic fields from waveguide antennas, in particular when estimating field levels in regions near the aperture for the purpose of protection against radiation hazards.

The paper is organized as follows. The theoretical framework upon which the analysis is based is presented in Sec. 2. The formulations presented in Sec. 2 are applied to derive expressions for fields radiated from OECW antennas in Sec. 3. Results and discussion are included in Sec. 4 and conclusion in Sec. 5.

2. Theoretical Development

The computation of the radiated fields from a range of canonical antennas that are characterized by a circular symmetry in their geometry depends on the evaluation of the integral

$$Q_{u,v} = \frac{1}{2\pi}\int_{\rho_1}^{\rho_2}\int_0^{2\pi} \rho'^{v+1} \begin{matrix}\cos\\ \sin\end{matrix} u\phi' \frac{\mathrm{e}^{-\mathrm{j}\beta R_0}}{R_0}\mathrm{d}\phi'\mathrm{d}\rho' \quad (1)$$

in which u and v are integers and their sum is even. β is the wave number and R_0 is the distance between the field point (ρ, ϕ, z) in the space surrounding the antenna and the source point (ρ', ϕ', z') on the antenna. R_0 can be expressed as

$$R_0 = \sqrt{R^2 - 2\rho'\rho\cos(\phi - \phi')} \quad (2)$$

where

$$R = \sqrt{(z - z')^2 + \rho^2 + \rho'^2}. \quad (3)$$

The integral in (1) can be evaluated analytically as in the following analysis.
Let $Q_{u,v}$ in (1) be written in the form

$$Q_{u,v} = \int_{\rho_1}^{\rho_2} \rho'^{v+1} I_u(\rho')\mathrm{d}\rho' \quad (4)$$

where

$$I_u(\rho') = \frac{1}{2\pi}\int_0^{2\pi} \begin{matrix}\cos\\ \sin\end{matrix} u\phi' \frac{\mathrm{e}^{-\mathrm{j}\beta R_0}}{R_0}\mathrm{d}\phi'. \quad (5)$$

The scalar Green's function $\mathrm{e}^{-\mathrm{j}\beta R_0}/R_0$ in (5) may be expanded using the Lommel expansions [11] as

$$\frac{\mathrm{e}^{-\mathrm{j}\beta R_0}}{R_0} = -\mathrm{j}\beta\sum_{v=0}^{\infty}\frac{(\beta^2\rho\rho')^v}{v!}\frac{h_v^{(2)}(\beta R)}{(\beta R)^v}\cos^v(\phi - \phi'). \quad (6)$$

Subsitituting $\mathrm{e}^{-\mathrm{j}\beta R_0}/R_0$ from (6) into (5), yields

$$I_u(\rho') = -\mathrm{j}\beta\sum_{v=1}^{\infty}\frac{(\beta^2\rho\rho')^v}{v!}\frac{h_v^{(2)}(\beta R)}{(\beta R)^v} I_{u,v} \quad (7)$$

where

$$I_{u,v} = \frac{1}{2\pi}\int_0^{2\pi}\cos^v(\phi - \phi') \begin{matrix}\cos\\ \sin\end{matrix} u\phi'\mathrm{d}\phi'. \quad (8)$$

Using the substitution $\psi = \phi' - \phi$ along with the fact that the integral of $\cos^k\psi \sin u\psi$ with respect to ψ from 0 to 2π is zero, (8) reduces to

$$I_{u,v} = K_{u,v} \begin{matrix}\cos\\ \sin\end{matrix} u\phi' \quad (9)$$

where

$$K_{u,v} = \frac{1}{2\pi}\int_0^{2\pi}\cos^v\psi\cos u\psi\mathrm{d}\psi. \quad (10)$$

$K_{u,v}$ in (10) can be obtained [12] as

$$K_{u,v} = \begin{cases}\frac{1}{2^v}\frac{v!}{p!(v-p)!}, & u \le v, \text{ and } v - u = 2p\\ 0, & \text{otherwise}\end{cases}. \quad (11)$$

Using (11) along with (9), (7) becomes

$$I_u(\rho') = -\mathrm{j}\beta \begin{matrix}\cos\\ \sin\end{matrix} u\phi' \sum_{p=0}^{\infty}\frac{(\beta^2\rho\rho'/2)^{2p+u}}{p!(p+u)!}\frac{h_{2p+u}^{(2)}(\beta R)}{(\beta R)^{2p+u}}. \quad (12)$$

Substituting $I_u(\rho')$ from (12) back into (4), yields

$$Q_{u,v} = -\mathrm{j}\beta \begin{matrix}\cos\\ \sin\end{matrix} u\phi \sum_{p=0}^{\infty}\frac{(\beta^2\rho/2)^{2p+u}}{p!(p+u)!}\zeta_{u,v,p} \quad (13)$$

where

$$\zeta_{u,v,p} = \int_{\rho_1}^{\rho_2}\frac{h_{2p+u}^{(2)}(\beta R)}{(\beta R)^{2p+u}}\rho'^{2p+u+v+1}\mathrm{d}\rho'. \quad (14)$$

Since $u + v$ is even, (14) can be rewritten as

$$\zeta_{u,v,p} = \int_{\rho_1}^{\rho_2}\frac{h_{2p+u}^{(2)}(\beta R)}{(\beta R)^{2p+u}}\rho'^{2(p+s)+1}\mathrm{d}\rho' \quad (15)$$

where $u + v = 2s$, $(s = 0, 1, 2, \ldots)$. Using the substitution

$$f = \rho'^{2(p+s)}, \qquad dg = -\beta^2\rho'\frac{h_{2p+u}^{(2)}(\beta R)}{(\beta R)^{2p+u}}\mathrm{d}\rho' \quad (16)$$

and integrating (15) by parts [13], yields

$$\zeta_{u,v,p} = -\frac{h_{2p+u-1}^{(2)}(\beta R)}{(\beta R)^{2p+u-1}}\frac{\rho'^{2(p+s)}}{\beta^2}\Bigg|_{\rho_1}^{\rho_2} - \frac{2(p+s)}{\beta^4}\int_{\rho_1}^{\rho_2}(-\beta^2\rho')\frac{h_{2p+u-1}^{(2)}(\beta R)}{(\beta R)^{2p+u-1}}\rho'^{2(p+s-1)}\mathrm{d}\rho'. \quad (17)$$

Repeating the above steps, we can obtain finally

$$\zeta_{u,v,p} = \frac{2^{p+\frac{u+v}{2}}(p+\frac{u+v}{2})!}{\beta^{2(p+\frac{u+v}{2}+1)}} \frac{h^{(2)}_{p+u-\frac{u+v}{2}-1}(\beta R_1)}{(\beta R_1)^{p+u-\frac{u+v}{2}-1}} - \frac{2^{p+\frac{u+v}{2}}(p+\frac{u+v}{2})!}{\beta^{2(p+\frac{u+v}{2}+1)}} \frac{h^{(2)}_{p+u-\frac{u+v}{2}-1}(\beta R_2)}{(\beta R_2)^{p+u-\frac{u+v}{2}-1}} - \sum_{k=0}^{p+\frac{u+v}{2}-1} \frac{(p+\frac{u+v}{2})!}{(p+\frac{u+v}{2}-k)!} \frac{2^k \rho_2^{2(p+\frac{u+v}{2}-k)}}{\beta^{2(k+1)}} \cdot \left[\frac{h^{(2)}_{2p+u-k-1}(\beta R_2)}{(\beta R_2)^{2p+u-k-1}} - \left(\frac{\rho_1}{\rho_2}\right)^{2(p+\frac{u+v}{2}-k)} \frac{h^{(2)}_{2p+u-k-1}(\beta R_1)}{(\beta R_1)^{2p+u-k-1}} \right] \tag{18}$$

where $R_1 = \sqrt{r^2+\rho_1^2}$, $R_2 = \sqrt{r^2+\rho_2^2}$, and $r = \sqrt{(z-z')^2+\rho^2}$. Substituting $\zeta_{u,v,p}$ from (18) into (13) completes the exact solution of integrals in (1). This solution can be applied to determine the radiated fields from a range of antennas such as circular aperture antennas, circular waveguide antennas, and antennas of circular symmetry, provided that the condition on u and v stated in (1) has been satisfied, which is the case for most practical circular aperture antennas.

3. Application to Circular Waveguides

In this section, (18) is applied to obtain exact expressions for the fields radiated from the aperture of an OECW erected on an infinite perfect electric conducting ground plane.

3.1 The Vector Potential

Consider an OECW of radius a mounted on an infinite ground plane as shown in Fig. 1. Assuming a TE$_{mn}$ mode time-varying fields characterized by the time factor $e^{+j\omega t}$, ($j = \sqrt{-1}$, ω is the angular frequency, and t is time), propagating in the waveguide, the spatial components of the electric field $\mathbf{E}_a$ in the cylindrical coordinates at any point ($\rho' \le a, \phi'$) on the surface of the waveguide aperture can be expressed as [14]

$$E_\rho = V_{mn} \frac{m J_m(\alpha\rho')}{\rho'} \sin m\phi', \tag{19}$$

$$E_\phi = V_{mn} \frac{\partial J_m(\alpha\rho')}{\partial \rho'} \cos m\phi'. \tag{20}$$

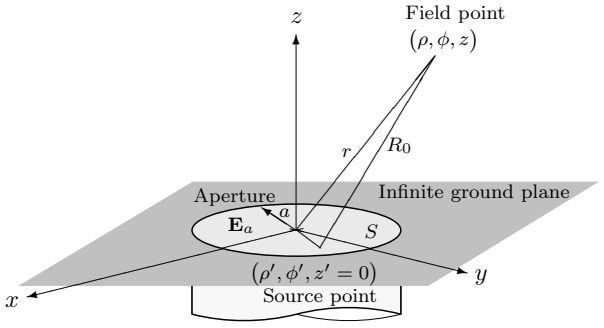


Fig. 1. Geometry of the problem.

V_{mn} is a constant, $J_m(\cdot)$ is the Bessel function of the first kind of order m, $\alpha = \chi'_{mn}/a$, and χ'_{mn} is the nth non-zero root of the derivative of the mth order Bessel function. Transforming E_ρ and E_ϕ to the rectangular coordinate system and applying the equivalence principle with the image theory, it can be shown that the components of the magnetic current density $\mathbf{M}$ on the surface of the aperture are given by

$$\begin{bmatrix} M_x \\ M_y \end{bmatrix} = V_{mn}\alpha \begin{bmatrix} +\cos(m-1)\phi' & -\cos(m+1)\phi' \\ -\sin(m-1)\phi' & -\sin(m+1)\phi' \end{bmatrix} \begin{bmatrix} J_{m-1}(\alpha\rho') \\ J_{m+1}(\alpha\rho') \end{bmatrix}. \tag{21}$$

Thus, the electric vector potential $\mathbf{F}$ can be obtained from

$$\mathbf{F} = \frac{\varepsilon}{4\pi} \iint_S \mathbf{M} \frac{e^{-j\beta R_0}}{R_0} dS' \tag{22}$$

where ε is permittivity of the surrounding medium. Using (19)–(21) with $dS' = \rho' d\phi' d\rho'$, it can be shown that the x-component of $\mathbf{F}$ in (22) is

$$F_x = \frac{\varepsilon V_{mn}\alpha}{4\pi} \int_{\rho_1}^{\rho_2} \int_0^{2\pi} d\phi' d\rho' \frac{e^{-j\beta R_0}}{R_0} \rho' \cdot \begin{cases} -2J_1(\alpha\rho')\cos\phi', & m = 0 \\ J_{m-1}(\alpha\rho')\cos(m-1)\phi' - J_{m+1}(\alpha\rho')\cos(m+1)\phi', & m > 0 \end{cases}. \tag{23}$$

Using (1) along with the series representation of Bessel function $J_n(\cdot)$ [15, p.360], F_x in (23) can be written as

$$F_x = \varepsilon V_{mn} \sum_{q=0}^{\infty} \frac{(-1)^q}{q!} \begin{cases} -2G_q^{0n}, & m = 0 \\ G_q^{mn}, & m > 0 \end{cases} \tag{24}$$

where

$$G_q^{0n} = \frac{(\frac{\chi'_{0n}}{2a})^{2q+2}}{(q+1)!} Q^c_{1,2q+1} \tag{25}$$

$$G_q^{mn} = \frac{(\frac{\chi'_{mn}}{2a})^{2q+m}}{(q+m-1)!} \left[Q^c_{m-1,2q+m-1} - \frac{(\frac{\chi'_{mn}}{2a})^2}{(q+m)(q+m+1)} Q^c_{m+1,2q+m+1} \right] \tag{26}$$

$$Q^c_{u,v} = -j\beta \cos u\phi \sum_{p=0}^{\infty} \frac{(\beta^2\rho/2)^{2p+u}}{p!(p+u)!} \zeta_{u,v,p}. \tag{27}$$

For a waveguide of radius a, $\rho_1 = 0$, $\rho_2 = a$, $R_1 = \sqrt{z^2+\rho^2} = r$, and $R_2 = \sqrt{z^2+\rho^2+a^2} = r_a$. Hence, from (18) $\zeta_{u,v,p}$ becomes

$$\zeta_{u,v,p} = \frac{2^{p+\frac{u+v}{2}}(p+\frac{u+v}{2})!}{\beta^{2(p+\frac{u+v}{2}+1)}} \frac{h^{(2)}_{p+u-\frac{u+v}{2}-1}(\beta r)}{(\beta r)^{p+u-\frac{u+v}{2}-1}} - \sum_{k=0}^{p+\frac{u+v}{2}} \frac{(p+\frac{u+v}{2})!}{(p+\frac{u+v}{2}-k)!} \frac{2^k a^{2(p+\frac{u+v}{2}-k)}}{\beta^{2(k+1)}} \frac{h^{(2)}_{2p+u-k-1}(\beta r_a)}{(\beta r_a)^{2p+u-k-1}} \tag{28}$$

Using (25) and (26) with (24), F_x can be written as

$$F_x = -j\beta\varepsilon V_{mn} \sum_{q=0}^{\infty} \sum_{p=0}^{\infty} \frac{(-1)^q}{q!p!} \begin{cases} -2X_{qp}^{0n}\cos\phi, & m = 0 \\ X_{qp}^{mn}, & m > 0 \end{cases} \tag{29}$$

where

$$X_{qp}^{0n} = \frac{\left(\frac{\chi'_{0n}}{2a}\right)^{2q+2}}{(q+1)!}\frac{(\beta^2\rho/2)^{2p+1}}{(p+1)!}\zeta_{1,2q+1,p} \tag{30}$$

$$X_{qp}^{mn} = \frac{\left(\frac{\chi'_{mn}}{2a}\right)^{2q+m}}{(q+m-1)!}\frac{(\beta^2\rho/2)^{2p+m-1}}{(p+m-1)!}\left[\cos(m-1)\phi\zeta_{m-1,2q+m-1,p} - \frac{\cos(m+1)\phi\left(\frac{\chi'_{mn}}{2a}\right)^2}{(q+m)(q+m+1)}\frac{(\beta^2\rho/2)^2\zeta_{m+1,2q+m+1,p}}{(p+m)(p+m+1)}\right]. \tag{31}$$

Similarly, it can be shown that the y-component of $\mathbf{F}$ is

$$F_y = \mathrm{j}\beta\varepsilon V_{mn}\sum_{q=0}^{\infty}\sum_{p=0}^{\infty}\frac{(-1)^q}{q!p!}\begin{cases}2X_{qp}^{0n}\sin\phi, & m=0\\ Y_{qp}^{mn}, & m>0\end{cases} \tag{32}$$

where

$$Y_{qp}^{mn} = \frac{\left(\frac{\chi'_{mn}}{2a}\right)^{2q+m}}{(q+m-1)!}\frac{(\beta^2\rho/2)^{2p+m-1}}{(p+m-1)!}\left[\sin(m-1)\phi\zeta_{m-1,2q+m-1,p} + \frac{\sin(m+1)\phi\left(\frac{\chi'_{mn}}{2a}\right)^2}{(q+m)(q+m+1)}\frac{(\beta^2\rho/2)^2\zeta_{m+1,2q+m+1,p}}{(p+m)(p+m+1)}\right]. \tag{33}$$

The vector potential components F_x and F_y obtained in (29) and (32) are exact and valid everywhere in free space region surrounding the aperure of the waveguide.

3.2 The Electromagnetic Fields

The electromagnetic fields are related to $\mathbf{F}$ by

$$\mathbf{E} = -\frac{1}{\varepsilon}\nabla\times\mathbf{F} \tag{34}$$

$$\mathbf{H} = -\frac{1}{\mathrm{j}\omega\mu}\nabla\times\mathbf{E}. \tag{35}$$

Substituting F_x and F_y from (29) and (32) respectively, into (34) with extensive algebraic manipulations, the electric field components radiated from a TE$_{mn}$ mode waveguide antenna shown in Fig. 1 can be expressed as

$$E_x = \begin{cases}E_x^{0n}\cos\phi, & m=0\\ E_x^{mn}, & m>0\end{cases} \tag{36}$$

$$E_y = \begin{cases}-E_x^{0n}\sin\phi, & m=0\\ E_y^{mn}, & m>0\end{cases} \tag{37}$$

$$E_z = \begin{cases}0, & m=0\\ E_z^{mn}, & m>0\end{cases} \tag{38}$$

where

$$E_x^{0n} = -\mathrm{j}2\beta^2 z V_{mn}\sum_{q=0}^{\infty}\sum_{p=0}^{\infty}\frac{(-1)^q}{q!p!}\frac{\left(\frac{\chi'_{0n}}{\beta a}\right)^{2q+2}}{(q+1)!}\frac{(\beta\rho)^{2p+1}}{(p+1)!}\gamma_{pq} \tag{39}$$

$$E_x^{mn} = -\mathrm{j}\beta^2 z V_{mn}\sum_{q=0}^{\infty}\sum_{p=0}^{\infty}(-1)^q\frac{\left(\frac{\chi'_{mn}}{\beta a}\right)^{2q+m}}{q!(q+m-1)!}\frac{(\beta\rho)^{2p+m-1}}{p!(p+m-1)!}\cdot\left[A_{mpq}\sin(m-1)\phi + C_{mnpq}B_{mpq}\sin(m+1)\phi\right] \tag{40}$$

$$E_y^{mn} = -\mathrm{j}\beta^2 z V_{mn}\sum_{q=0}^{\infty}\sum_{p=0}^{\infty}(-1)^q\frac{\left(\frac{\chi'_{mn}}{\beta a}\right)^{2q+m}}{q!(q+m-1)!}\frac{(\beta\rho)^{2p+m-1}}{p!(p+m-1)!}\cdot\left[A_{mpq}\cos(m-1)\phi - C_{mnpq}B_{mpq}\cos(m+1)\phi\right] \tag{41}$$

$$E_z^{mn} = -\mathrm{j}V_{mn}\frac{\sin m\phi}{\rho}\sum_{q=0}^{\infty}\sum_{p=0}^{\infty}(-1)^q\frac{\left(\frac{\chi'_{mn}}{\beta a}\right)^{2q+m}}{q!(q+m-1)!}\frac{(\beta\rho)^{2p+m-1}}{p!(p+m-1)!}\cdot\left\{(\beta\rho)^2\left[A_{mpq}+C_{mnpq}B_{mpq}\right] - 2(p+m-1)U_{mpq} - 2(p+m+1)C_{mnpq}W_{mpq}\right\}. \tag{42}$$

The coefficients γ_{pq}, A_{mpq}, B_{mpq}, C_{mnpq}, U_{mpq}, and W_{mpq} are given by

$$\gamma_{pq} = \frac{(p+q+1)!}{2^{p+q+2}}\frac{h_{p-q}^{(2)}(\beta r)}{(\beta r)^{p-q}} - \sum_{k=0}^{p+q+1}\frac{(p+q+1)!}{(p+q+1-k)!}\cdot\frac{(\beta a/2)^{2q-k+1}}{2^{k+1}}\left(\frac{a}{2r_a}\right)^{2p-k+1}h_{2p-k+1}^{(2)}(\beta r_a) \tag{43}$$

$$A_{mpq} = \frac{(p+q+m-1)!}{2^{p+q+m}}\frac{h_{p-q}^{(2)}(\beta r)}{(\beta r)^{p-q}} - \sum_{k=0}^{p+q+m-1}\frac{(p+q+m-1)!}{(p+q+m-1-k)!}\cdot\frac{(\beta a/2)^{2q+m-k-1}}{2^{k+1}}\left(\frac{a}{2r_a}\right)^{2p+m-k-1}h_{2p+m-k-1}^{(2)}(\beta r_a) \tag{44}$$

$$B_{mpq} = \frac{(p+q+m+1)!}{2^{p+q+m+2}}\frac{h_{p-q}^{(2)}(\beta r)}{(\beta r)^{p-q}} - \sum_{k=0}^{p+q+m+1}\frac{(p+q+m+1)!}{(p+q+m+1-k)!}\cdot\frac{(\beta a/2)^{2q+m-k+1}}{2^{k+1}}\left(\frac{a}{2r_a}\right)^{2p+m-k+1}h_{2p+m-k+1}^{(2)}(\beta r_a) \tag{45}$$

$$C_{mnpq} = \frac{\left(\chi'_{mn}\frac{\rho}{a}\right)^2}{(q+m)(q+m+1)(p+m)(p+m+1)} \tag{46}$$

$$U_{mpq} = \frac{(p+q+m-1)!}{2^{p+q+m}}\frac{h_{p-q-1}^{(2)}(\beta r)}{(\beta r)^{p-q-1}} - \sum_{k=0}^{p+q+m-1}\frac{(p+q+m-1)!}{(p+q+m-1-k)!}\cdot\frac{(\beta a/2)^{2q+m-k}}{2^{k+1}}\left(\frac{a}{2r_a}\right)^{2p+m-k-2}h_{2p+m-k-2}^{(2)}(\beta r_a) \tag{47}$$

$$W_{mpq} = \frac{(p+q+m+1)!}{2^{p+q+m+2}}\frac{h_{p-q-1}^{(2)}(\beta r)}{(\beta r)^{p-q-1}} - \sum_{k=0}^{p+q+m+1}\frac{(p+q+m+1)!}{(p+q+m+1-k)!}\cdot\frac{(\beta a/2)^{2q+m+2-k}}{2^{k+1}}\left(\frac{a}{2r_a}\right)^{2p+m-k}h_{2p+m-k}^{(2)}(\beta r_a). \tag{48}$$

The corresponding magnetic fields can be optained by substituting E_x, E_y, and E_z from (36)–(38) into (35).

3.3 On-Axis Fields

On the axis of the aperture $\rho = 0$, $r = z$, and $r_a = \sqrt{z^2 + a^2}$. Substituting $\rho = 0$ into (36)–(38) results in $E_x^{0n} = E_x^{mn} = E_z^{mn} = 0$, while $E_y^{mn} \neq 0$ for $m = 1$, hence, $E_x = E_z = 0$ and E_y reduces to

$$E_y = -\mathrm{j}\beta^2 z V_{1n} \sum_{q=0}^{\infty} \frac{(-1)^q}{q!} \left(\frac{\chi'_{1n}}{2\beta a}\right)^{2q+1} D_q \tag{49}$$

where

$$D_q = (2\beta z)^q h_{-q}^{(2)}(\beta z) - \sum_{k=0}^{q} \frac{(\beta a)^{2q-k}}{(q-k)!} \left(\frac{2r_a}{a}\right)^k h_{-k}^{(2)}(\beta r_a). \tag{50}$$

This result reveals that for an OECW the axial fields result only from the modes with $m = 1$ and there are no contributions from the other modes with $m \neq 1$. This conclusion was previously pointed out in [6].

3.4 Dominant Mode Fields

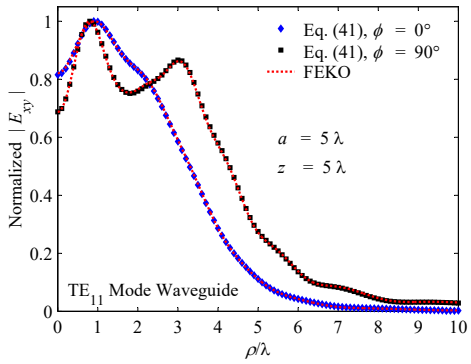
For a dominant mode (TE_{11}), $m = n = 1$ and $\chi_{11} = 1.841$. Hence, the fields radiated from a TE_{11} mode OECW antenna can be obtained from general expressions (36)–(48) by substituting $m = 1$ and $\chi_{11} = 1.841$ as

$$E_x = -\mathrm{j}\beta^2 z V_{11} \sin 2\phi \sum_{q=0}^{\infty} \sum_{p=0}^{\infty} (-1)^q \frac{\left(\frac{1.841}{\beta a}\right)^{2q+2}}{q!(q+2)!} \frac{(\beta\rho)^{2p+2}}{p!(p+2)!} B_{1pq} \tag{51}$$

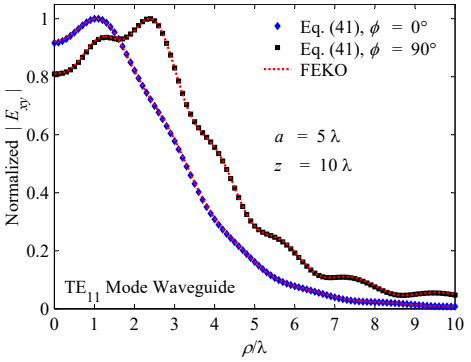
$$\begin{aligned} E_y = &-\mathrm{j}\beta^2 z V_{11} \sum_{q=0}^{\infty} \sum_{p=0}^{\infty} (-1)^q \frac{\left(\frac{1.841}{\beta a}\right)^{2q+1}}{q!q!} \frac{(\beta\rho)^{2p}}{p!p!} A_{1pq} \\ &+ \mathrm{j}\beta^2 z V_{11} \cos 2\phi \sum_{q=0}^{\infty} \sum_{p=0}^{\infty} (-1)^q \frac{\left(\frac{1.841}{\beta a}\right)^{2q+2}}{q!(q+2)!} \frac{(\beta\rho)^{2p+2}}{p!(p+2)!} B_{1pq} \end{aligned} \tag{52}$$

$$\begin{aligned} E_z = &-\mathrm{j}V_{mn} \frac{\sin\phi}{\rho} \sum_{q=0}^{\infty} \sum_{p=0}^{\infty} (-1)^q \frac{\left(\frac{1.841}{\beta a}\right)^{2q+1}}{q!q!} \frac{(\beta\rho)^{2p}}{p!p!} \\ &\cdot \left\{(\beta\rho)^2 \left[A_{1pq} + C_{11pq} B_{1pq}\right] - 2\left[pU_{1pq} + (p+2)C_{11pq} W_{1pq}\right]\right\}. \end{aligned} \tag{53}$$

In the above expressions, which apply to the dominant mode waveguides, the summation over the index q can be truncated after the first three terms only without a significant error provided that $\beta a \gg 1.841$ ($a \gg 0.3\lambda$, where λ is the wavelength) and $\beta\rho > 1$.

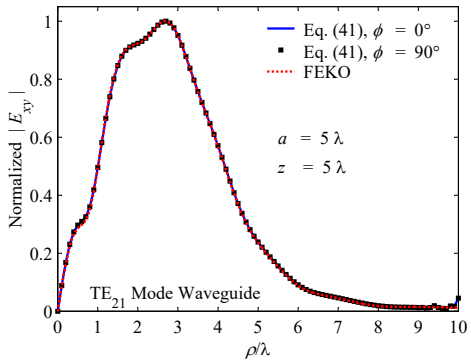


(a) $z = 5\lambda$

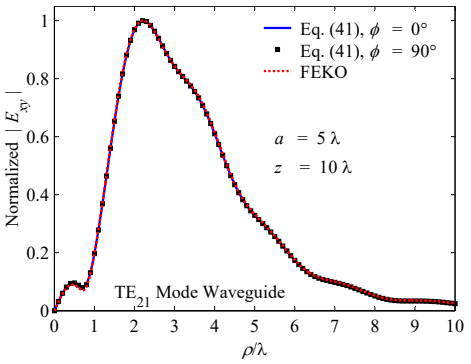


(b) $z = 10\lambda$

Fig. 2. E_{xy} in the near-field region of an OECW with TE_{11} mode fields.



(a) $z = 5\lambda$



(b) $z = 10\lambda$

Fig. 3. E_{xy} in the near-field region of an OECW with TE_{21} mode fields.

4. Results and Discussion

4.1 Validation of the Solution

The electric field $E_{xy} = \sqrt{|E_x|^2 + |E_y|^2}$ radiated from an OECW of radius $a = 5\lambda$ with TE_{11} and TE_{21} modes was computed in the near -field regions in the planes $\phi = 0°$ and $\phi = 90°$, in the range $0 \le \rho/\lambda \le 10$, at heights $z = 5\lambda$ and $z = 10\lambda$ using (41) and (42) and displayed in Figs. 2 and 3. The results agree well with the corresponding ones obtained from FEKO simulation software. The simulation procedure has been explained in Appendix A.

The axial fields of an OECW of radius $a = 2\lambda$ with TE_{11} mode fields were computed from (49) and compared to the results extracted from [7, Fig. 3(a)] and corresponding results obtained from FEKO as shown in Fig. 4. The agreement between the three sets of results is clear.

The above results of comparisons show clearly that the field expressions presented in this paper are in excellent agreement with the published results and those obtained using FEKO, which reveals the validity of these expressions.

4.2 Convergence of the Solution

To study the convergence of the field expressions (36)–(38), E_y is computed and plotted against θ in the range $0 \le \theta \le \pi/2$ for a TE_{11} mode circular waveguide of radius $a = 5\lambda$ on the surface of the sphere $r = 10\lambda$ as shown in Fig. 5. The computation is carried out taking $V_{11} = 1.0\,\mathrm{V}$ while the summations are truncated after the first $M+1$ terms ($M = 1, 2, 10$) for the summation over the index q and $N+1$ terms ($N = 5, 10, 20, 40$) for that over the index p.

It is clear that from Fig. 5 the convergence slows down towards $\theta = \pi/2$ (towards the source). This due to the fact that the integrand in (1) suffer a sigularity when $R_0 \to 0$ (when the field point approaches the source point) due to the presence of the kernel $\exp[-j\beta R_0]/R_0$. Nevertheless, it remains integrable, which has enabled us to obtain a solution to the problem under study through direct integration, without the need for approximations or the elimination of these singularities.

Moreover, the summation over q converges very rapidly compared to that over p, which is obvious for this TE_{11} mode case since $\beta a \gg \chi_{11}$ while $\beta\rho$ is large. This true for all other modes as long as $\beta a \gg \chi_{mn}$.

In general, the solution's convergence becomes slower as r increases. For very large values of r, a computational overflow might occur prior to obtaining the solution. This makes the field expressions presented in this paper more appropriate and computationally efficient for near-field regions, ranging from the antenna surface to the Fresnel zone, while still preserving mathematical validity in all regions.

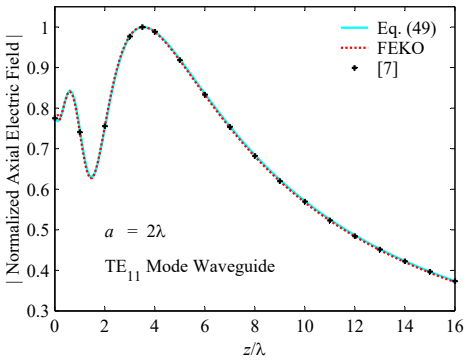
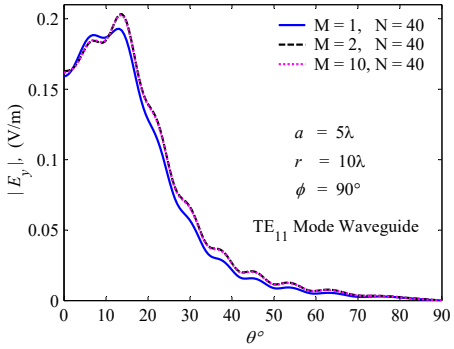
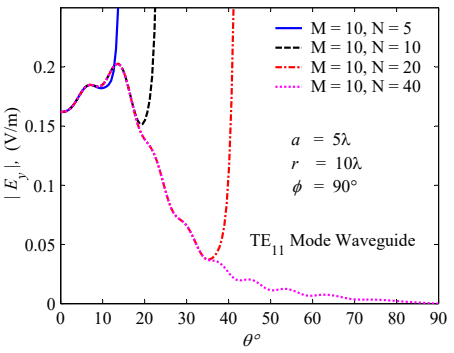


Fig. 4. Axial near-fields of an OECW of radius $a = 2\lambda$ with TE_{11} mode fields propagating in it compared to the results extracted from [7, Figure 3(a)] and corresponding results obtained from FEKO.



(a) M = 1, 2, 10 and N = 40



(b) M = 10 and N = 5, 10, 20, 40

Fig. 5. Convergence of the solution.

4.3 Axial Near-Fields

Using (49), the axial electric fields in the near-field region for an open-ended circular waveguide with $m = 1$ and $n = 1, 2, 3, 4, 5$ are computed and displayed in Fig. 6. The radius of the waveguide is $a = 10\lambda$, $V_{1n} = 1.0\,\mathrm{V/m}$ and it is known that $\chi_{1n} = 1.841, 5.3315, 8.5363, 11.7060, 14.8636$ for the respective values of n above.

The results shown in Fig. 6 indicate that the amplitude of the axial fields rises with n in the reactive near-field region close to the aperture surface, while the amplitude envelope of the oscillations (originating from the diffracted fields) decreases as n increases provided that for all cases $V_{1n} = 1.0\,\mathrm{V/m}$.

4.4 General Remarks

Based on the formulas derived in this paper and in light of the results mentioned above, we can draw the following remarks regarding the behaviour of electromagnetic fields near the aperture of a TE_{mn} mode waveguide antenna:

- The general field expressions (36)–(42) reduce to more simple ones along the orthogonal axes $\phi = 0°$ (the $y = 0$ plane) and $\phi = 90°$ (the $x = 0$ plane) based on the value of m as summarized in Tab. 1.
- Based upon the above point, the dominant mode (TE_{11}) field $E_{xy} = \sqrt{|E_x|^2 + |E_y|^2}$ vary differently in the planes $\phi = 0°$ and $\phi = 90°$ with spatial variables. In general, for all even m, the field E_{xy} has an identical magnitude in both the $\phi = 0°$ and $\phi = 90°$ planes, while for odd m, its characteristics differ between them. This is clear from Figs. 2 and 3 for the cases of TE_{11} and TE_{21} modes.
- On the axis of the waveguide all the electric field components vanish except E_y. Furthermore, it is observed that the axial fields arise solely from the modes with $m = 1$, and there is no contribution from the other modes, as clear from (49), which agrees with [6].
- In the near field region and not very close to the waveguide axis, the magnitude of the electric field component E_z is always much less than $E_{xy} = \sqrt{|E_x|^2 + |E_y|^2}$. Fig. 7 displays some examples (including TE_{11}, TE_{21}, TE_{13}, and TE_{32} modes) revealing this fact.
- The paper focused on determining and analysing the electric fields; however, using the same analysis described above and (35), the corresponding magnetic fields can be determined.

5. Conclusion

Grasping the radiated electromagnetic fields in the near-field of waveguide antennas is essential for numerous applications. This paper derives excat formulas for the radiated fields of an open-ended circular waveguide antenna of arbitrary size and mode in a unified approach. The methodology depends on analytical techniques without using approximations. The results derived from these formulas align remarkably well with related published findings and those acquired through commercial software, confirming their correctness. These expressions are more appropriate and computationally efficient for the near-field up to the Fresnel region, although they can be mathematically applied throughout the space above the waveguide aperture plane. These field expressions can be applied to assess the level of electromagnetic fields radiated from circular waveguide antennas in the near field regions for the purpose of protection against radiation hazards.

Although the paper addresses the radiated fields of OECW; however, the analysis can be applied to a wide range of antennas featuring circular apertures.

ϕ	$m = 0$	$m = 1, 3, \cdots$	$m = 2, 4, \cdots$
0°	$E_x \neq 0$, $E_y = E_z = 0$	$E_y \neq 0$, $E_x = E_z = 0$	$E_y \neq 0$, $E_x = E_z = 0$
90°	$E_y \neq 0$, $E_x = E_z = 0$	$E_x = 0$, $E_y \neq 0, E_z \neq 0$	$E_x \neq 0$, $E_y = E_z = 0$

Tab. 1. Electric field components in the x- and y-planes.

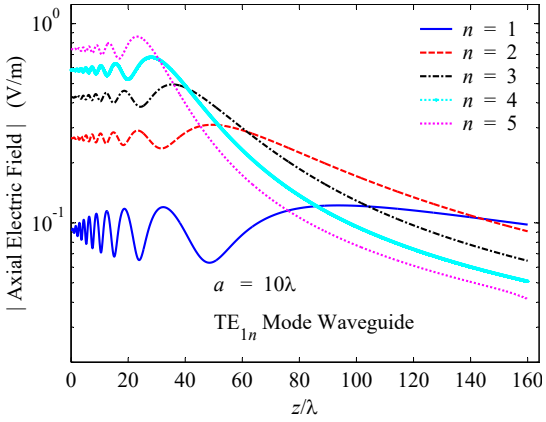
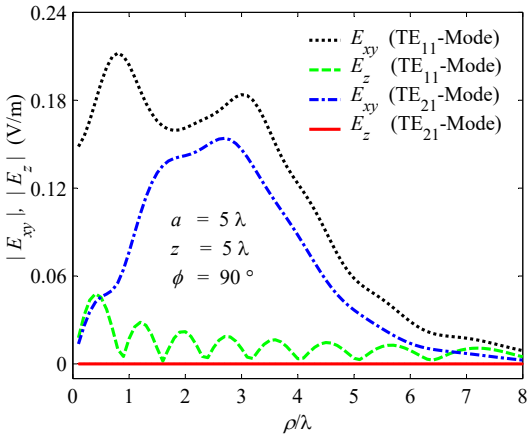
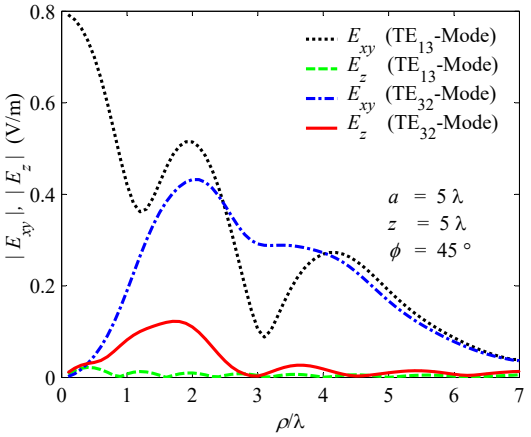


Fig. 6. Axial near-fields of an OECW of radius $a = 10\lambda$ with TE_{1n} mode fields propagating in it.



(a) TE_{11}, TE_{21} modes fields in the plane $\phi = 90°$



(b) TE_{13}, TE_{32} modes fields in the plane $\phi = 45°$

Fig. 7. Comparizon between E_z and $E_{xy} = \sqrt{|E_x|^2 + |E_y|^2}$.

References

[1] POU, Z. A., SHAFAI, L. Analytical models of dual-polarized primary matched feeds for offset reflector antennas with low cross-polarization properties at both asymmetry and diagonal planes. *IEEE Transactions on Antennas and Propagation*, 2016, vol. 64, no. 5, p. 1627–1633. DOI: 10.1109/TAP.2016.2537361

[2] RAMZI, M. R., ABOU-KHOUSA, M., PRAYUDI, I. Near-field microwave imaging using open-ended circular waveguide probes. *IEEE Sensors Journal*, 2017, vol. 17, no. 8, p. 2359–2366. DOI: 10.1109/JSEN.2017.2669301

[3] NEPA, P., BUFFI, A. Near-field-focused microwave antennas: Near-field shaping and implementation. *IEEE Antennas and Propagation Magazine*, 2017, vol. 59, no. 3, p. 42–53. DOI: 10.1109/MAP.2017.2686118

[4] BALANIS, C. A. Evolution of antenna technology: Apertures, waveguides, horns, and Vivaldi. *IEEE Antennas and Propagation Magazine*, 2024, vol. 66, no. 6, p. 29–38. DOI: 10.1109/MAP.2024.3428920

[5] DASH, T., PRINSLOO, D., YAROVOY, A. Radiation from the open-ended over-moded cylindrical waveguide. In *4th URSI Atlantic Radio-Science Conference (AT-RASC)*. Gran Canaria (Spain), 2024, p. 1–4. DOI: 10.46620/ursiatrasc24/qeut4611

[6] CICCHETTI, R., FARAONE, A. Analysis of open-ended circular waveguides using physical optics and incomplete Hankel functions formulation. *IEEE Transactions on Antennas and Propagation*, 2007, vol. 55, no. 6, p. 1887–1892. DOI: 10.1109/TAP.2007.895639

[7] CICCHETTI, R. Radiation from open-ended circular waveguides: A formulation based on the incomplete Hankel functions. *Progress in Electromagnetics Research*, 2008, vol. 78, p. 285–300. DOI: 10.2528/PIER07091405

[8] DANIELE, V., ZICH, R. *The Wiener-Hopf Method in Electromagnetics*. Edison, NJ (USA): SciTech Publishing, 2014, p. 279–297. DOI: 10.1049/SBEW503E

[9] LE-WEI, L., MOOK-SENG, L., PANG-SHYAN, K., et al. Radiation of an aperture antenna covered by a spherical-shell chiral radome and fed by a circular waveguide. *IEEE Transactions on Antennas and Propagation*, 1998, vol. 46, no. 5, p. 664–671. DOI: 10.1109/8.668909

[10] SHANKPAL, P., ARUR, V., KADAMBI, G., et al. A generalized approach for computation of near field radiation pattern of an antenna. *International Journal of Antennas and Propagation*, 2014, vol. 2014, p. 1–18. DOI: 10.1155/2014/958148

[11] WANG, W.-X. The exact kernel for cylindrical antenna. *IEEE Transactions on Antennas and Propagation*, 1991, vol. 39, no. 4, p. 434–435. DOI: 10.1109/8.81454

[12] WERNER, D. H. On a new cylindrical harmonic representation for spherical waves. *IEEE Transactions on Antennas and Propagation*, 1999, vol. 47, no. 1, p. 97–100. DOI: 10.1109/8.752999

[13] HAMED, S. M., ALSAIF, H. An exact series solution of fields radiated from a magnetic frill source using Lommel expansions. *IEEE Access*, 2024, vol. 12, p. 89353–89362. DOI: 10.1109/ACCESS.2024.3419693

[14] LI, S., ZHU, Z. A numerical method to determine mode content in circular waveguide based on an integral identity equation. *Applied Mathematical Modelling*, 2012, vol. 36, p. 2926–2934. DOI: 10.1016/j.apm.2011.09.067

[15] ABRAMOWITZ, M., STEGUN, I. A. *Handbook of Mathematical Functions*. New York, NY (USA): Dover, 1972

[16] HAMED, S. M. TE11_waveguide-NearFields [software repository]. GitHub. Available at: https://github.com/alihamed707-spec/TE11_waveguide-NearFields

About the Author ...

Sameir HAMED received the B.Sc. degree in Electrical Engineering from the University of Khartoum, Khartoum, Sudan, in 1991. He received the M.Sc. degree from the University of Jordan, Amman, Jordan, in 1998, and the Ph.D. degree from the Karary University, Omdurman, Sudan, in 2012, both in telecommunications. He is currently an Assistant Professor with the University of Hail, Hail, Kingdom of Saudi Arabia. From 1994 to 2017, he was with the Faculty of Engineering and Technology, Nile Valley University, Atbara, Sudan. He is the author of two books: Electromagnetics for Engineering Students (Bentham Science Publishers, 2017) and Principles of Antenna Engineering (Lulu.com, 2016). His research interests include, theoretical and computational electromagnetics, antenna theory, and electromagnetic wave propagation.

Appendix A: Simulation of M

To perform FEKO simulation, the current distribution on the surface of the waveguide aperture **M** was modeled by an array of infinitesimal magnetic dipoles. The current strength of each is determined by the field distribution at the respective locations of the dipoles according to (19) and (20). the separation between any adjacent dipoles was $\lambda/8$ which gives quite good results. The model of the current distribution is generated by a program developed in the FEKO editor. An example of a simulated current distribution on the aperture surface of an open-ended waveguide is shown in Fig. 8.

The source code (Feko script) that generates the current distribution in Fig. 8 along with a MATLAB code for computing the electric field E_y are available at a GitHub repository via the link given in [16].

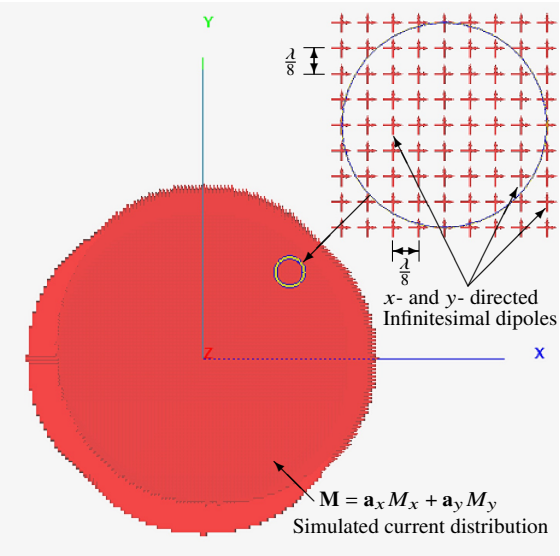


Fig. 8. Simulation of the current distribution on the surface of the waveguide aperture in FEKO.